



## Arrhythmia as a Result of Poor Intercellular Coupling in the Sinus Node: A Simulation Study

PER ÖSTBORN\*†, BJÖRN WOHLFART‡ AND GUNNAR OHLÉN\*

\*Departments of Mathematical Physics, Lund University, S-221 00 Lund, Sweden and

‡Clinical Physiology, Lund University, S-221 00 Lund, Sweden

(Received on 12 June 2000; Accepted in revised form on 24 April 2001)

The effects of reduced intercellular coupling in the sinus node were investigated by means of simulations. Coupling was reduced both uniformly, and by introducing localized interaction blocks. In either case, model sinus node element networks typically splitted into frequency domains. These were defined as groups of neighbour elements which all attained the same mean firing frequency. In systems, simulating the vicinity of an impulse outlet to the atrium, the sinus node elements often splitted into two domains, one slowly firing just inside the outlet, and one normally firing large domain in the sinus node interior. This two-domain situation was analysed using a two-element system. Wenckebach conduction and advanced ( $m:1$ ) exit blocks were seen, together with more odd block patterns and slow chaotic rhythms. The two-domain situation appeared also when two discrete outlets were considered. The slow domains around each outlet synchronized via the atrium. However, if there were some degree of exit block through one of the outlets only, brady-tachy like rhythms could be simulated due to a re-entrant circuit including both sinus node and atrial tissue. In conclusion, poor coupling in the sinus node seems to be sufficient to produce most arrhythmias in the sick sinus syndrome

© 2001 Academic Press

### 1. Introduction

In this study, we investigated which clinically significant cardiac arrhythmias can appear because of poor intercellular coupling in the sinus node (SN). We aimed to obtain a qualitative picture, not to give parameter values at which different phenomena appear.

Patients suffering from arrhythmia originating in the SN area are said to have the “sick sinus syndrome” (Rubenstein *et al.*, 1972; Ferrer, 1973; Kaplan *et al.*, 1973; Jordan *et al.*, 1978; Delon

*et al.*, 1992). In this syndrome, sinus rhythm is most often slower than normal, but there may be paroxysmal attacks of tachycardia or atrial fibrillation. The latter situation is called the brady-tachy syndrome. The slow rhythms may be either periodic or aperiodic. By a periodic rhythm we mean a sequence of firing intervals that finally repeats itself. The periodic rhythms are called sino-atrial (SA) exit blocks. These include, for example, Wenckebach conduction and advanced ( $m:1$ ) block. Slow aperiodic rhythms are called sinus arrest rhythms.

There is convincing evidence that the cells in the SN entrain their frequencies because of the electric coupling which is mediated by gap

† Author to whom correspondence should be addressed.  
E-mail: [per.ostborn@matfys.lth.se](mailto:per.ostborn@matfys.lth.se)

junctions (De Haan, 1982; Jalife, 1984; Delmar *et al.*, 1986). Cai *et al.* (1993) have studied the complex dynamics arising in a pair of model SN cells with different natural frequencies when this coupling is reduced. Examples of Wenckebach rhythms and slow aperiodic rhythms in weakly coupled model SN cells have been obtained previously by Michaels *et al.* (1986).

We studied the activity of poorly coupled SN cells in an atrium with both simple and more complex models, in order to test the generality of the observed phenomena, and to gain an understanding of the dynamics. The paper is organized along a line of progressive simplification. First, we studied a network model of the vicinity of an impulse exit site to the atrium. This model included some ultrastructural qualities suggested by experiments. We investigated the effects both of a uniform gap junction conductance decrease, and of the introduction of electrically insulating connective tissue strands. The same types of arrhythmias were produced in either case. Then we investigated a more schematic network model in which the influence of the atrium was replaced by a constant leakage current. The leakage arises because the maximum diastolic potential (MDP) of SN cells is less negative than the atrial cell resting potential. The same arrhythmias were seen in this model. The SN elements often splitted into two frequency domains, one normally firing interior domain, and one slow peripheral. This allowed the use of only two SN elements, one of which suffered from a strong leakage current. The bifurcation diagram resulting from changing coupling strength was studied in detail. Again, the same arrhythmias were seen. Owing to their seeming generality, in an accompanying paper, we attempt to explain the rhythms and bifurcations of this system using circle maps based on phase response curves. Model systems including two SN exit sites showed the same type of dynamics as those with a single exit site, but also a kind of re-entry including both SN and atrial tissue. This might be one mechanism behind the brady-tachy syndrome.

Severe sinus arrhythmia, as simulated in this study, can only appear *in vivo* if the leakage current to the atrium makes it impossible for the SN cells close to the SA junction to drive the atrium properly without help from the SN

interior. Leakage reduces the firing frequency since diastolic depolarization becomes slower. It is also assumed in the simulations that the border between the SN and the atrium is sharp, and specifically that the impulse leaves the SN at discrete exit sites. The validity of these assumptions is discussed in Section 4.

## 2. Methods

The Irisawa & Noma (1982) model was used to simulate SN elements. This is a Hodgkin & Huxley (1952)-type membrane model based on voltage clamp measurements on aggregates of rabbit SN cells. Five currents ( $i_{Ca}$ ,  $i_K$ ,  $i_{Na}$ ,  $i_h$  and  $i_b$ ) contribute to the total current  $I$  flowing across the cell membrane. To save computation time, the Na-channel was removed, and the Ca-channel activation variable  $d$  was set to its steady-state value  $d_\infty$ . These operations are justified since the Na-current stays very small throughout the limit cycle, and  $d$  adjusts very quickly to  $d_\infty$ .

To produce a frequency variation among elements, the membrane densities of Ca- and K-current channels were altered, both with the same factor  $Q$  compared to their normal values. Frequency increased with  $Q$ , and the waveform changed in a way similar to that recorded by Boyett *et al.* (1999) when they studied differences in spontaneous activity between central and peripheral parts of the rabbit SN. The model used is specified in Appendix A.

Non-automatic (atrial) elements were simulated with the membrane model developed by Wohlfart & Ohlén (1999). The equations defining this model are also given in Appendix A.

The gap junction current  $j_{kl}$  from cell  $k$  to a neighbour cell  $l$  was described as  $j_{kl} = g_{kl} (V_k - V_l)$ , with a constant conductance  $g_{kl}$ . Here  $V_k$  is the membrane potential of cell  $k$ . Thus,  $V_k$  followed  $dV_k/dt = -(I_k + \sum_l j_{kl})/C_k$ , where  $I_k$  is the current flowing across the cell membrane and  $C_k$  is the membrane capacitance. Cells were treated as two-dimensional squares, and were coupled to neighbours  $l$  having a common edge.

Since a large amount of data was to be collected, we aimed to use the quickest possible integration method in each case. To integrate the

systems in Figs 1 and 4–8, the forward Euler method was used. For the two-element system (Figs 5 and 6) the time step was set to 1 ms, otherwise 0.5 ms was used. For the systems in Figs 2 and 3, we used the integration method of Victorri *et al.* (1985). In this method, voltage changes are controlled in each step. Such a method had to be used because the large leakage currents across the SA junction contributed to fast voltage changes of the small peripheral SN elements. This made the Euler algorithm diverge, unless very small time steps were used. In our version of the Victorri method, if the voltage change  $|\Delta V|$  of *any* element exceeded 0.5 mV, the time step  $\Delta t$  was halved and calculations were redone. If  $|\Delta V| < 0.5$  mV for *all* elements,  $\Delta t$  was doubled in *the next* iteration.  $\Delta t$  was initially set to 0.5 ms, and was not allowed to exceed this value.

In all simulations, measurements were started after sufficiently long time so that no transient

dynamics was recorded. After that, the dynamics always seemed independent of initial conditions. However, this was not systematically investigated.

### 3. Results

#### 3.1. FREQUENCY DOMAINS

Figure 1 shows results of simulations with a network of  $20 \times 20$  SN elements. In panel (a) these were not coupled, so that the mean firing intervals were the same as the natural intervals. These were distributed according to a gradient with a superposed smaller random variation. Values of  $Q$  (Section 2) were assigned according to  $Q = 0.8 + ((k - 1)/19)^3 + r$ , where  $k$  is the row number, and  $r$  is a uniform random variable between 0 and 0.2. This produced natural intervals between 369 and 288 ms. This design was inspired by the experiments by Opthof *et al.* (1987) and Boyett *et al.* (1999), which demonstrated

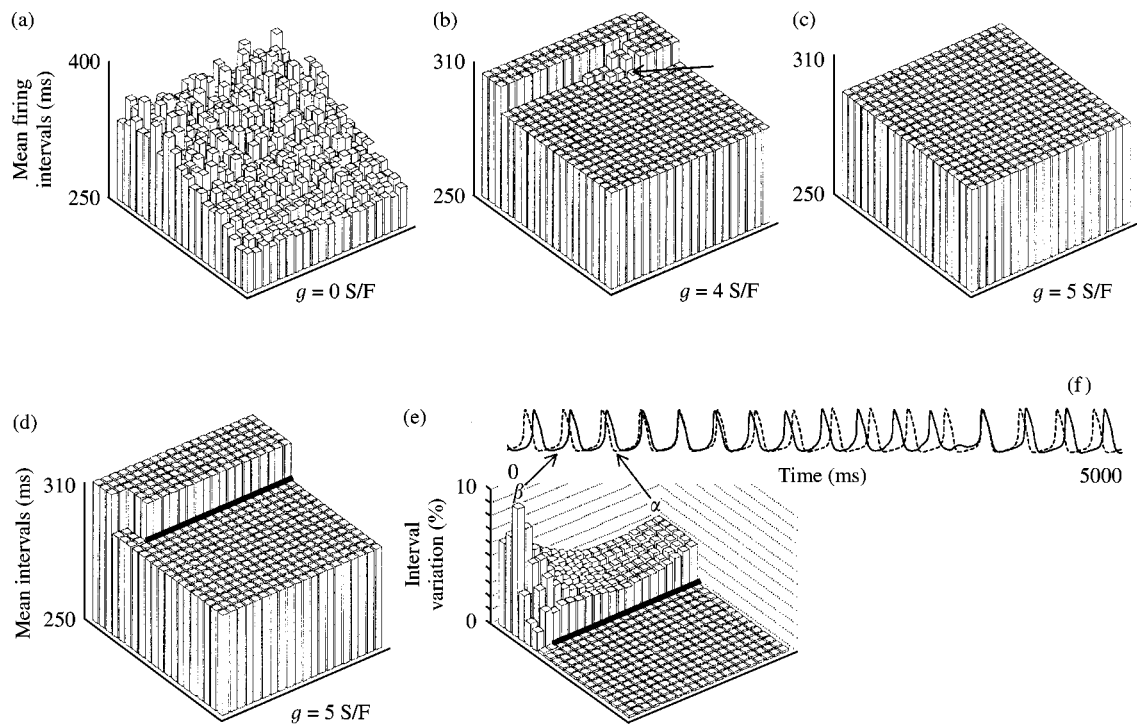


FIG. 1. Simulations of  $20 \times 20$  SN elements coupled homogeneously with conductance  $g$ . Natural intervals (a) were varied through a distribution of  $Q$  (Section 2). (b) Formation of six frequency domains for weak coupling. The element marked with an arrow is a domain of its own, since it has no nearest neighbours with the same frequency. A different scale is used in panels (b)–(d), so that the domains are easier to distinguish. (c) Frequency entrainment for higher coupling. (d) An interaction block (—) caused splitting into two domains of an entrained network. (e) Standard deviations of the mean intervals for the system in (d) divided by the mean intervals. (f) Potential traces of two elements marked in (e). The element far from the domain border fired more regularly than the element close to it.

a gradient with longer natural intervals in the rabbit SN centre (400–500 ms) than in the periphery towards the crista terminalis (CT) ( $\sim 300$  ms).

The introduction of a uniform coupling conductance  $g$ , caused frequency entrainment for  $g > 4.5$  S/F [panel (c)]. For lower values of  $g$ , frequency domains appeared. These were defined as groups of neighbour elements having identical mean frequencies. In panel (b), six domains can be recognized for a uniform conductance  $g = 4$  S/F.

The natural frequency gradient was approximately linear. Nevertheless, the fastest domain was substantially larger than the slower ones. This was seen in other simulations too (not shown), and thus seemed to be a general quality, at least of the present SN element model.

Panel (d) shows how an interaction block made an entrained system split into two domains [cf. with panel (c)]. The block could be interpreted as a strand of connective tissue, since these seem to be electrically insulating (De Mazière *et al.*, 1992). Frequency entrainment was regained at  $g = 5.7$  S/F.

The dynamics of the systems in panels (b) and (d) was aperiodic. This was typically the case when global frequency entrainment was absent. However, it could happen that the mean frequencies of all domains became rationally related, leading to periodic dynamics. This was seen mainly when there were only two domains.

Panel (e) shows the standard deviations of the firing intervals for the system in panel (d), in percent of the mean intervals. The slower domain showed larger interval variations. The interval variations were greatest close to the border between the domains, and tended to decrease with the distance from this border. This was seen in other simulations too (not shown), and thus seemed to be a general quality. Panel (f) shows potential traces of the elements  $\alpha$  and  $\beta$  marked in panel (e). The firings of  $\alpha$  were much more regular than those of  $\beta$ . This finding suggests that if the splitting into domains is to have any clinical significance, it has to occur close to the SA junction. Otherwise, atrial intervals would probably be quite regular. This is one reason why we focused our attention on the dynamics of SN cells close to the SA border.

### 3.2. NETWORK MODEL OF THE VICINITY OF A SINUS NODE IMPULSE EXIT SITE TO THE ATRIUM

Figure 2(a) shows the system under consideration. It is intended to incorporate some ultrastructural qualities suggested by experiments. Atrial cells are bigger than SN cells (James, 1977; Denyer & Brown, 1990; Verheijck *et al.*, 1998). To obtain a simple two-dimensional geometry, the non-automatic element capacitance (area) was set 4 times higher than the SN element capacitance. The thick lines represent electric insulation between nodal and atrial tissue. This design is motivated by the study by ten Velde *et al.* (1995), which indicated that the atrium forms narrowing strands penetrating into the SN, and that SN cells are coupled to atrial cells only at the tips of these strands. The coupling between the shaded SN elements was set 10 times higher than the coupling  $g_{SS}$  between the other SN elements. Microscope studies by Bleeker *et al.* (1980) indicated that intercellular coupling is greater in the peripheral parts of the SN close to the CT. Kwong *et al.* (1998) found that SN cells that stained for the gap junction protein Cx43 were arranged in bundles. In some sections, these were seen to abut atrial cells. Coppens *et al.* (1999) found that Cx43 was present in the rabbit SN only in a restricted zone near the border to the CT, which is the preferential pathway out of the SN (Cx40 and Cx45 were present throughout the node). These results suggest that SN cells close to outlets to the atrium indeed are more strongly coupled. The natural intervals of the SN elements were made to vary between 336 and 303 ms, due to a uniform random probability distribution of  $Q$  between 1 and 1.4. Since the system was only intended to model an SN tissue around an exit site, we did not include the full frequency gradient between the SN centre and periphery (Ophhof *et al.*, 1987; Verheijck *et al.*, 1998), nevertheless some random cell-to-cell variations are bound to exist. The coupling  $g_{SA}$  between SN and non-automatic elements was set to 100 S/F, and the coupling  $g_{AA}$  between non-automatic elements to 500 S/F (siemens per unit SN element capacitance in both cases). We refer to Section 4 for a discussion of these values.

Potential traces of the marked elements  $\alpha$ ,  $\beta$ , and  $\gamma$  are shown in panels (b)–(e). The leakage

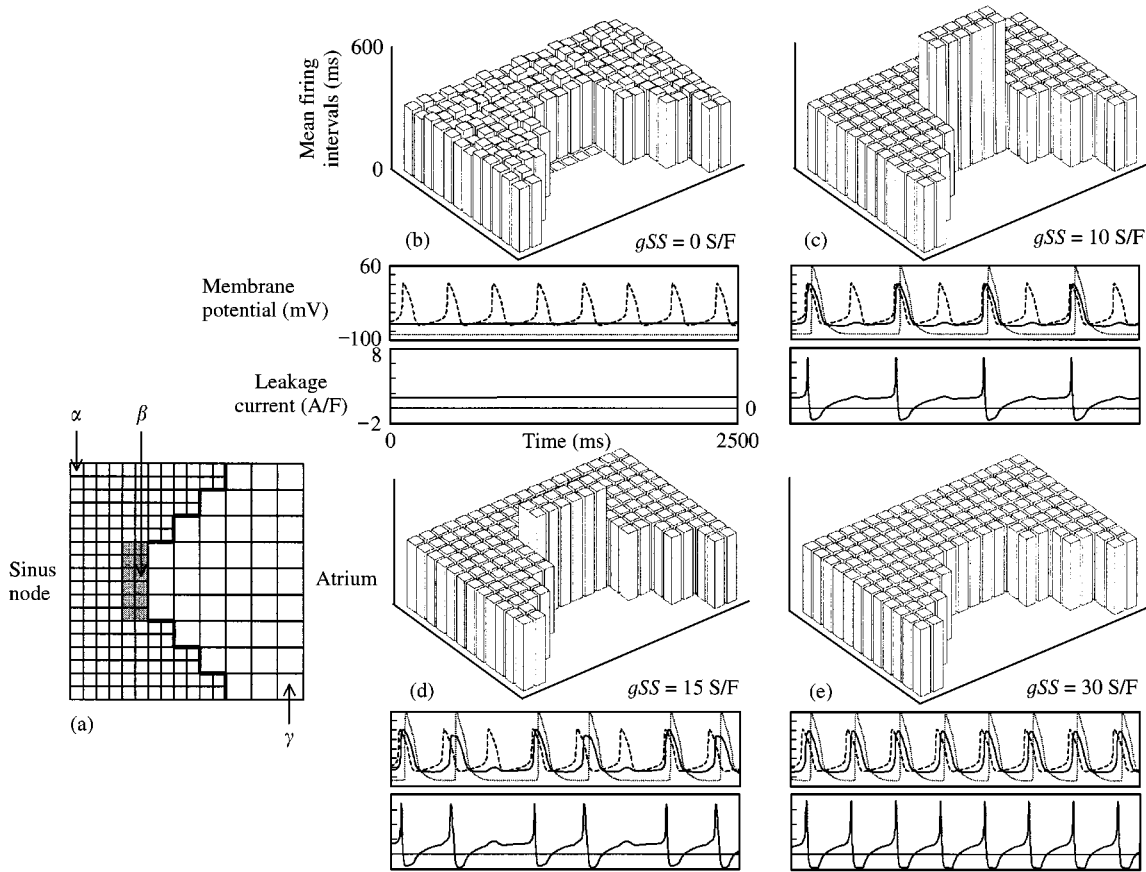


FIG. 2. Dynamics of a system modelling the neighbourhood of an SN exit site. (a) System architecture. The thick lines represent interaction blocks. The shaded SN elements are 10 times more strongly coupled than the other SN cells. Potential traces of the marked elements are shown in panels (b)–(e). For zero coupling ( $g_{SS}$ ) between SN elements, the six junctional SN elements did not fire as a result of the leakage (b). For  $g_{SS} > 21$  S/F, we had 1:1 conduction (e). For weaker coupling, exit blocks of various degrees appeared (c and d). Generally, the 12 shaded elements formed a slow domain, whereas the other SN elements fired normally. The leakage current flowing from element  $\beta$  to the atrium is shown in panels (b)–(e). (---)  $\alpha$ ; (—)  $\beta$ ; (····)  $\gamma$ .

current shown is the current flowing from element  $\beta$  to the non-automatic element in front. Panel (b) illustrates that for  $g_{SS} = 0$ , the six SA junctional SN elements were quiescent (no bars are shown). For  $g_{SS} = 10$  S/F, the SN tissue splitted into two domains, where the mean intervals of the 12 well-coupled junctional elements were twice that of the other elements [panel (c)]. A 2:1 advanced exit block was present. The notation  $m:n$  means that  $n$  out of  $m$  SN firings reach the atrium. For  $g_{SS} = 15$  S/F, the ratio of mean intervals between the junctional and interior SN elements was  $3/2$ , and a 3:2 Wenckebach rhythm was seen. All SN elements became frequency entrained for  $g_{SS} > 21$  S/F, leading to perfect impulse transmission to the atrium. The dynamics was periodic in all panels.

Figure 3 illustrates the effects of non-homogeneous coupling decrease in the SN part of the system in Fig. 2. Interaction blocks of various sizes and positions were introduced. These were intended to model strands of connective tissue, and are represented by thick lines.  $g_{SA}$  and  $g_{AA}$  were the same as in Figure 2.  $g_{SS}$  was set to 30 S/F in all panels, which led to frequency entrainment in the absence of the blocks [Fig. 2(e)]. In panels (a)–(d), a growing block, progressively decoupled the SN periphery from the interior. In panel (a), there was a 4:3 Wenckebach rhythm, in panel (b) an advanced 2:1 block, and in panel (c) a 5:2 exit block. The latter kind of rhythm will be discussed below, and also in the accompanying paper. Finally, in panel (d), a 3:1 block is seen. If the 12 well-coupled SN elements were completely

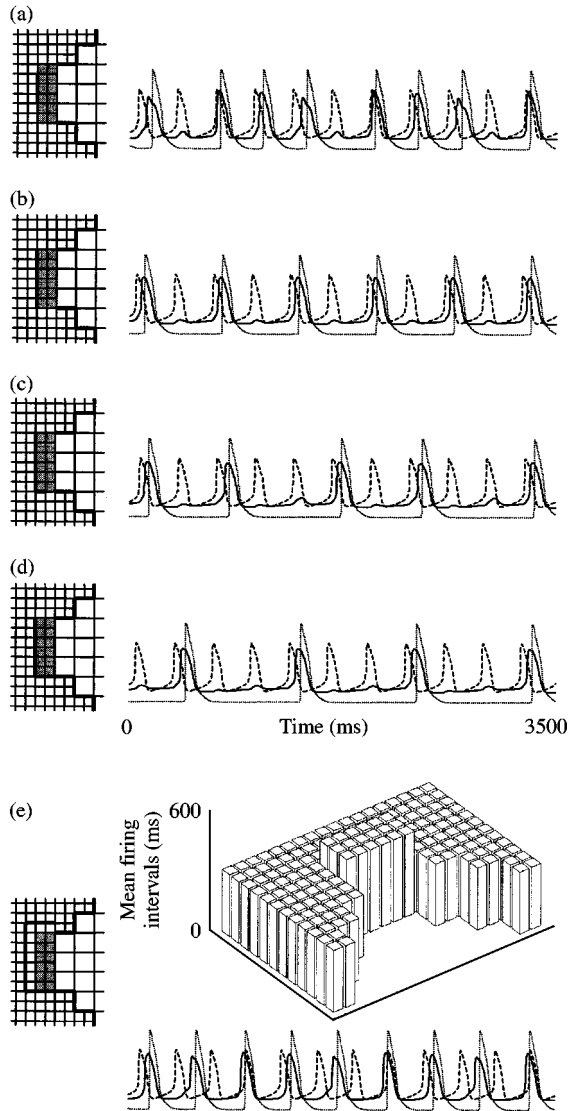


FIG. 3. Simulations with the same system as in Fig. 2, but with interaction blocks (connective tissue strands) inserted between SN elements.  $g_{SS} = 30$  S/F in all panels. Successive extension of a small strand produced more and more severe exit blocks. Potential traces from the same elements as in Fig. 2 are shown. (a) 4:3 conduction, (b) 2:1, (c) 5:2, and (d) 3:1. A block further inside the SN produced a larger, slow, junctional domain (e), and gave rise to 4:3 conduction.

decoupled from the rest of the SN tissue, a complete SA block developed (not shown). In all panels (a)–(d), a two-domain situation was present, with the 12 junctional elements forming the slower domain.

In panel (e), the block was placed a bit further away from the atrium. In this case, a larger junctional domain consisting of 18 elements

developed. As in panel (a) a 4:3 block was present. However, it was not of the Wenckebach type. Rather, the block created a “miniature SN” which was able to drive the atrium at a slightly lower, but quite regular rate. Blocks placed further inside the SN were not able to create conduction disorders.

The dynamics was periodic in all panels.

### 3.3. SIMPLIFIED NETWORK MODEL OF SINUS NODE TISSUE AROUND AN EXIT SITE

The influence of the atrium was replaced by a leakage current, and the geometry of the SN tissue was simplified. A constant leakage of 6 A/F was added to the four central elements in a network of  $10 \times 10$  elements [Fig. 4(b)]. These elements should be imagined to be placed around a discrete SN exit site [Fig. 4(a)]. For an isolated element, this leakage abolished spontaneous activity. As for the systems in Figs 2 and 3, each element was randomly assigned a  $Q$  value between 1 and 1.4. The coupling between the 16 most central elements were set 10 times higher than the coupling  $g$  between the other elements.

Figure 4(b)–(f) shows mean firing intervals for five different values of  $g$ . In panel (b) there were three frequency domains. The relation between their mean intervals was 6:3:2, giving a 3:1 block. In panel (c) there was a 2:1 block, and in panel (d) a 3:2 Wenckebach rhythm. In these panels, the elements fired periodically. Before entrainment settled (f), there was a region around  $g = 23$  S/F, in which some cells adjacent to the 16 central ones broke away from the large domain, and attained somewhat higher mean frequencies (e). The dynamics was aperiodic during this breakdown of the two-domain situation. Temporary exit blocks appeared at irregular intervals, as seen in panel (g).

### 3.4. A SINUS NODE WITH ONE EXIT SITE MODELLED AS A TWO-ELEMENT SYSTEM

Since states with only two domains occurred often, the dynamics during weak intra-nodal coupling was modelled with a two-element system. The similarity between the dynamics of the system in Figs 2 and 3 and that in Fig. 4, let us model the influence of the atrium as a leakage current. The SA blocks shown in Figs 2–4

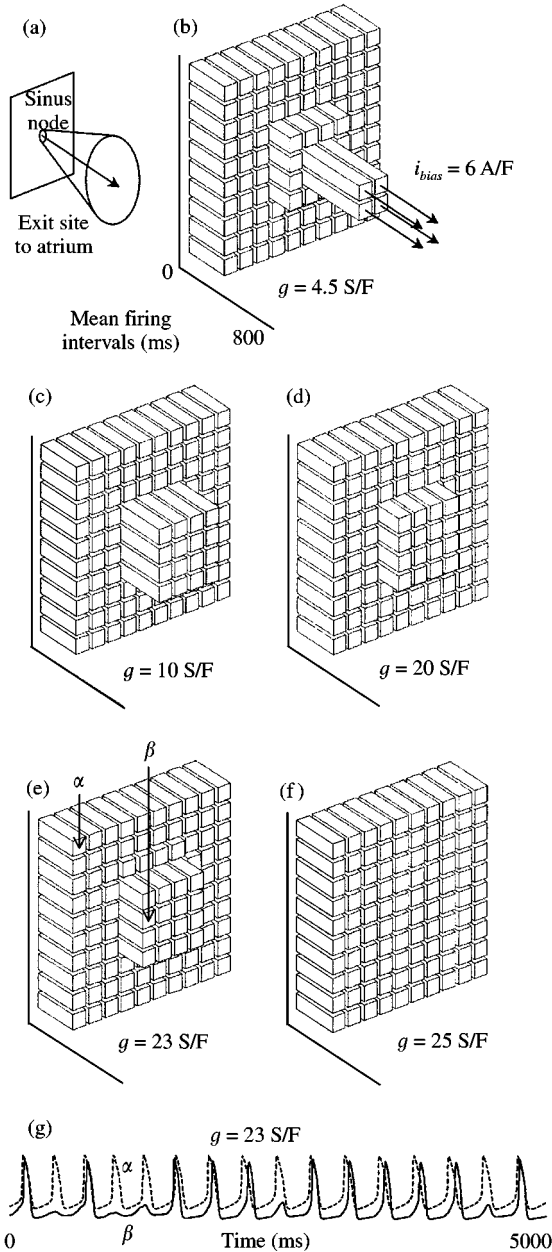


FIG. 4. Simulations of  $10 \times 10$  SN elements in a plane. The four central elements in the network suffered from a leakage current of  $6 \text{ A/F}$  and should be imagined to be placed around a discrete SN exit site. The coupling conductance between the 16 central elements was 10 times higher than the coupling  $g$  between the other elements. Natural frequencies were varied through a distribution of  $Q$  (Section 2). (a) Imagined position of the plane. (b)–(f) Mean firing intervals for each element for a sequence of increasing conductances  $g$ . (b) Three domains and 3:1 exit block. (c) Two domains and 2:1 block. (d) Two domains and 3:2 Wenckebach conduction. (e) Breakdown of the two-domain situation, leading to aperiodic dynamics. (f) Perfect frequency entrainment and 1:1 conduction. (g) Aperiodic block rhythm of the system in (e).

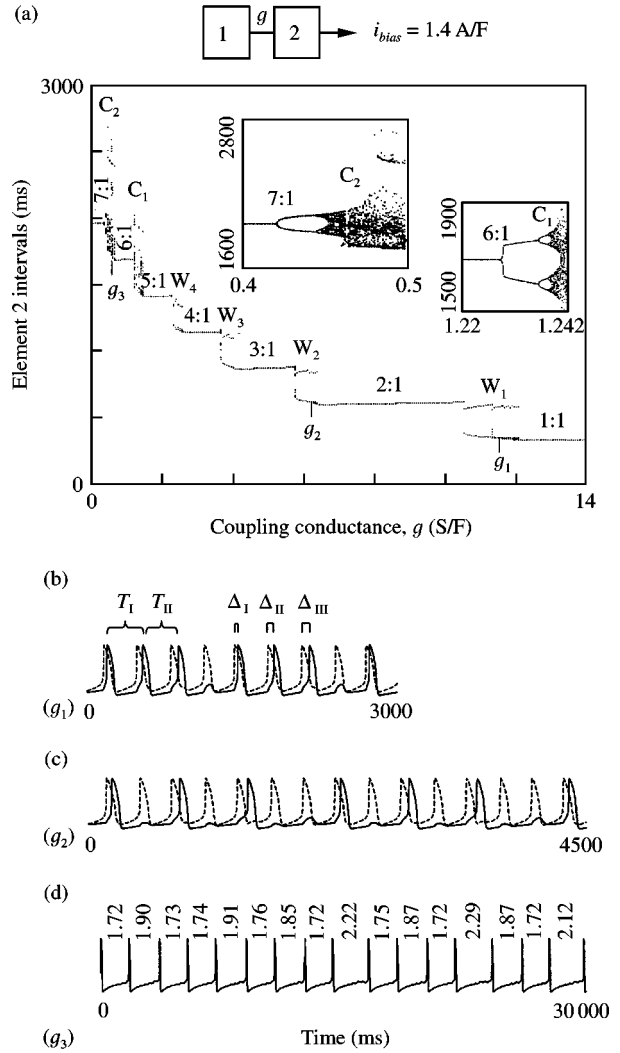


FIG. 5. Bifurcation diagram for a simplified two-element system in which element 2 suffered from a leakage current  $1.4 \text{ A/F}$ . The occurring firing intervals of element 2 are shown for different values of the coupling conductance  $g$ .  $m:1$  blocks occupy a great part of the diagram. Wenckebach rhythms were found in the region marked  $W_1$ . In the  $W_2$ – $W_4$  regions, other Wenckebach-like rhythms were found (see text). In the  $C_1$ - and  $C_2$ -regions the dynamics was chaotic. The insets show that these regions appeared after period-doubling cascades. (b) 4:3 Example of a Wenckebach rhythm at  $g_1 = 11.5 \text{ S/F}$ . The solid line corresponds to element 2.  $T_I = 347 \text{ ms}$ ,  $T_{II} = 344 \text{ ms}$ . (c) 7:3 rhythm from the  $W_2$  region at  $g_2 = 6.2 \text{ S/F}$ . (d) Chaotic rhythm from the  $C_2$  region at  $g_3 = 0.6 \text{ S/F}$ . Firing intervals are given in seconds.

appeared in such a simplified system also, and in the same order of appearance as coupling was altered.

We let element 2 suffer from the leakage  $1.4 \text{ A/F}$  [Fig. 5(a)]. This value is lower than in the

simplified network simulations (Fig. 4) since the element was intended to correspond to the entire slow junctional domain.  $g$  is the coupling conductance between the elements. Both elements had  $Q = 2$  (Section 2). In Fig. 5(a), the occurring firing intervals for element 2 at a given  $g$  are plotted against  $g$ . The firing intervals of element 1 (corresponding to the SN interior) increased only slightly from its uncoupled value 280 ms as  $g$  increased. The variance of its firing intervals was small irrespective of the dynamics of element 2.

In Fig. 5(a), plateaux on which every  $m$ -th firing of the interior element triggered the SA junctional one are seen.  $m$  increased in steps of one from 1 to 7 as  $g$  decreased. The widths of the plateaux decreased with increasing  $m$ .

Between the 1:1 and 2:1 conduction areas, Wenckebach rhythms arose. The region is marked  $W_1$ . In Fig. 5(b), a 4:3 rhythm is shown. The phase lag of the peripheral oscillator increased ( $\Delta_I < \Delta_{II} < \Delta_{III}$ ), and the firing interval decreased ( $T_I > T_{II}$ ), before one excitation was lost. These features are characteristic of Wenckebach conduction. In Fig. 6, the ratio  $R = m/n$  between the number of generated and conducted impulses in the  $W_1$  region is plotted against  $g$ .  $R(g)$  seemed to form a complete Devil's staircase (Ott, 1993), in which there are steps at each rational value between one and two. It is seen that the Wenckebach ratios  $(m + 1):m$  occupied most part of the parameter interval. The only other rhythm that occurred on an interval with appreciable width was 5:3 conduction. In the enlarged picture, the more exotic ratios 8:5 and 11:7 are also seen.

The rhythms in region  $W_2$  [Fig. 5(a)] were also Wenckebach-like. Here, at regular intervals, an additional firing was lost in a basic 2:1 cycle. In Fig. 5(c), such a 7:3 rhythm is shown. A 5:2 rhythm of this type is seen in Fig. 3(c). Generally,  $R = (2m + 1)/m$  for these rhythms. The characteristic increasing phase lags and decreasing intervals before the lost firing were seen in this case also. Analogously, in regions  $W_3$  and  $W_4$ , additional firings were lost at regular intervals in basic 3:1 and 4:1 rhythms. We had  $R = (3m + 1)/m$  and  $R = (4m + 1)/m$ , respectively.

The dynamics in regions  $C_1$  and  $C_2$  seemed to be chaotic. Both regions were entered via a

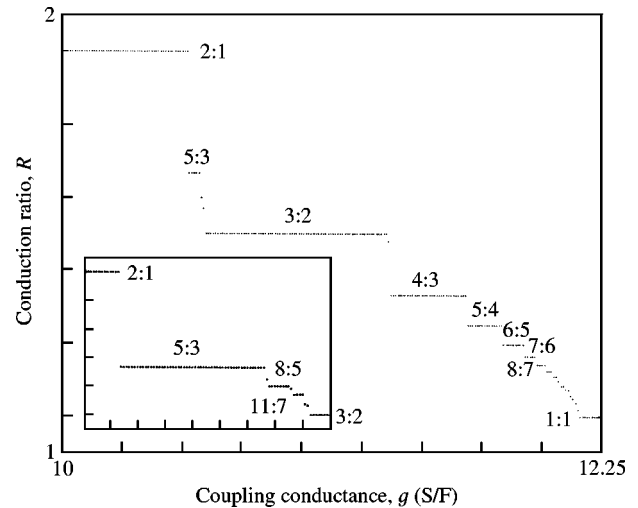


FIG. 6. The ratio  $R$  between the number of firings of elements 1 and 2 as a function of  $g$  in the Wenckebach region  $W_1$  in Fig. 5(a).  $R$  seems to form a Devil's staircase, with plateaux at all rationals between 1 and 2. The inset is an enlargement around the 5:3 region.

period-doubling cascade [see insets in Fig. 5(a)]. After the first branching in the 7:1 (6:1) region, every second firing interval of element 2 was a little bit longer. After the second branching four slightly different intervals occurred, then eight, and so on. By calculating the mean rate of exponential divergence of nearby trajectories in phase space, the Lyapunov exponents for  $g = 1.25$  ( $C_1$ ) and 0.6 S/F ( $C_2$ ) were estimated to be 0.32 and 0.45  $s^{-1}$ , respectively. Chaos is defined to be present then there is a positive exponent. In Fig. 5(d), a rhythm of element 2 for  $g_3 = 0.6$  S/F is shown, with firing intervals marked between the potential peaks. The most remarkable feature of these dynamical regimes is that some firing intervals were much longer than in the regular 6:1 and 7:1 regions which preceded them, respectively [Fig. 5(a)]. This is strange since the triggering impulses from element 1 were stronger. In the accompanying paper, we attempt to explain this and other qualities of the bifurcation diagram using phase response curves.

### 3.5. TAKING MULTIPLE SINUS NODE EXIT SITES INTO ACCOUNT

In order to find out whether the existence of two discrete outlets from the SN makes new types of rhythms possible, simulations were made with

a network of  $5 \times 10$  SN elements, in which two elements at some distance from each other suffered from leakage, simulating the exit sites. To be able to study the effects of the situation where the two outlets were surrounded by SN elements with different natural frequencies, a gradient of  $Q$  values (Section 2) was introduced [Fig. 7(a)].

In Fig. 7(b), it is seen that for  $g = 3$  S/F, the SN interior elements splitted into two domains, so that the two SA junctional elements were fed with different frequencies. Element  $\beta$  was locked in a 2:1 conduction ratio with respect to the firings of the surrounding domain, whereas no such relation existed for element  $\alpha$ . The overall dynamics was aperiodic. It seemed that all possible time delays between a firing of element  $\alpha$  and the next firing of element  $\beta$  occurred sometime (and vice versa). The last two qualities were typical when more than one interior domain was present.

For higher  $g$ , the interior elements formed a single domain [Fig. 7(c)]. If no  $Q$ -value gradient was used [Fig. 7(a)], this situation appeared at a very low  $g$  (not shown). In any case, both  $\alpha$  and  $\beta$  became frequency locked in a rational conduction ratio with respect to the common feeding frequency, and the dynamics became periodic. Thereafter, each drained element followed the sequence of bifurcations in the two-element system [Fig. 5(a)]. For a given  $g$ , they could be at different positions in the bifurcation diagram, depending on the  $Q$  values of  $\alpha$  and  $\beta$  and those of the surrounding elements. In Fig. 7(c),  $\alpha$  was in a 2:1 state and  $\beta$  showed 5:3 conduction.

Naively, the uncorrelated firings of  $\alpha$  and  $\beta$  at  $g = 3$  S/F indicate that long atrial activation intervals might alternate with very short ones. However, we have not taken into account that junctional elements at different outlets interact via the atrium. To this end, the system described in Fig. 8(a) was studied. The two interior SN elements allow dynamics corresponding to the splitting of the SN interior into more than one frequency domain [Fig. 7(b)].

It was found that whenever  $g_d$  was high enough to allow impulse conduction though the non-automatic elements, a firing of SN element 4 immediately triggered element 1 via the atrium, and vice versa. They achieved a common mean frequency and could be said to form a single domain. This corresponds to the unification of

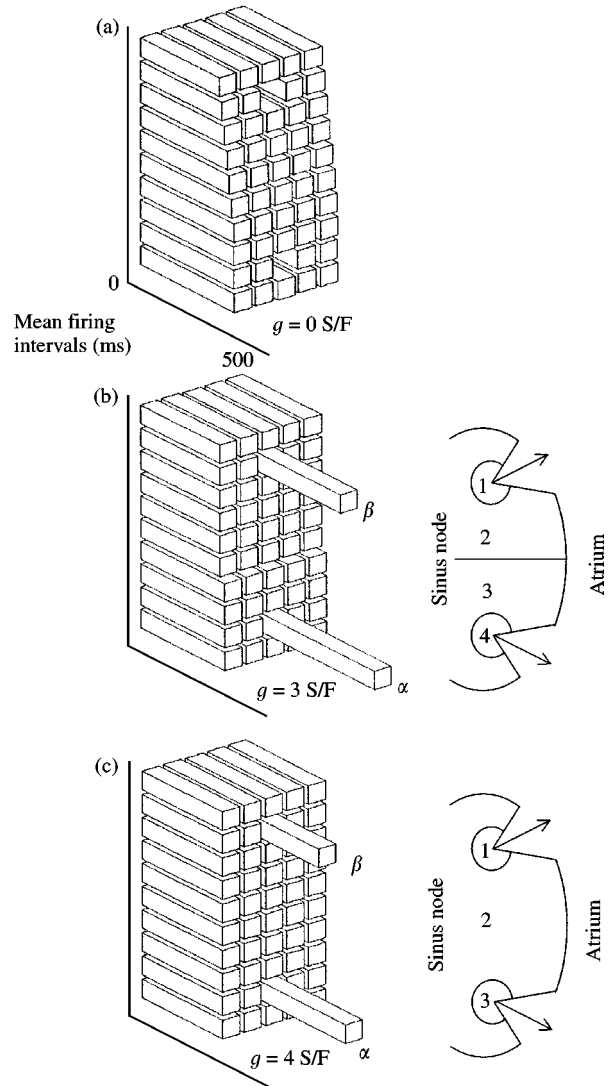


FIG. 7. Mean frequencies in a network of  $5 \times 10$  SN cells in which cell  $\alpha$  suffered from a leakage of 1.1 A/F and cell  $\beta$  of 1.4 A/F, simulating two discrete SN exit sites. Cells were coupled with a common conductance  $g$ . A gradient of  $Q$  values ranging from 1 to 2 with a superimposed minor random variation created a gradient in natural periods.  $Q(\alpha) = 1.5$ ,  $Q(\beta) = 1.7$ . (a)  $g = 0$  S/F. Since  $\alpha$  and  $\beta$  were quiescent, no bars are shown. (b)  $g = 3$  S/F. Four frequency domains remained; two interior ones (2 and 3) and two junctional (1 and 4), corresponding to cells  $\alpha$  and  $\beta$ . Both  $\alpha$  and  $\beta$  fired irregularly.  $\alpha$  was locked in a 2:1 conduction ratio with respect to the surrounding (irregularly firing) domain. (c)  $g = 4$  S/F. The SN interior constituted a single domain.  $\alpha$  was locked in a 2:1 state, and  $\beta$  showed 5:3 conduction. Periodic dynamics.

the junctional domains in Fig. 7(b) and (c). The junctional cell synchronization made impossible any atrial activation interval shorter than normal due to uncorrelated firings.

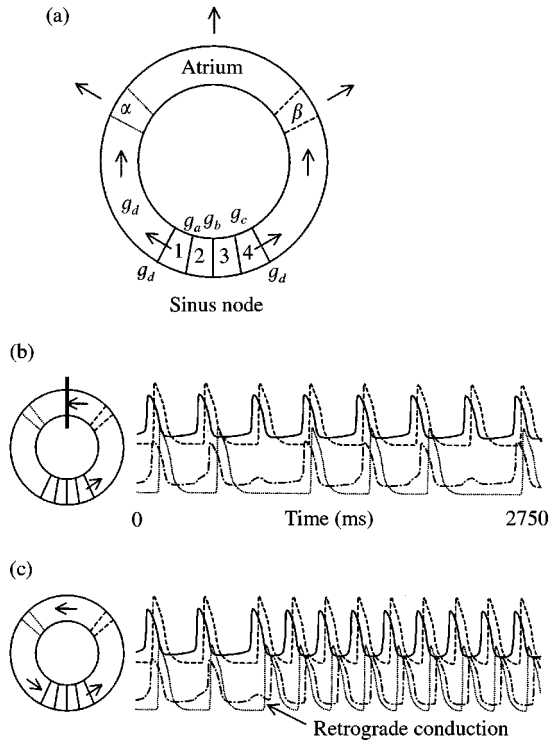


FIG. 8. (a) System used to study atrial rhythm when interactions via the atrium between SA junctional cells at different exit sites are taken into account. Four SN elements were used [cf. Fig. 7(b)]. The non-automatic elements were connected to a one-dimensional row.  $g_a$  was the coupling conductance between SN elements 1 and 2,  $g_b$  between 2 and 3, and  $g_c$  between elements 3 and 4. The same conductance  $g_d$  was used to couple one SN and one non-automatic element, and two non-automatic elements. (b) and (c) Proposed mechanism of brady-tachy rhythms. When the ring was disconnected in the atrial part, the right half fired normally whereas the left half showed 4:3 Wenckebach conduction (b). Action potentials of two non-automatic elements  $\alpha$  and  $\beta$  are displayed to show progression of the impulse. When an intact ring was used (c), the lost firing in the Wenckebach cycle enabled an impulse from the right to penetrate the SN retrogradely to the left, initiating re-entrant tachycardia. 30 Non-automatic elements were used. All elements in the ring had the same (unit) capacitance.  $Q_{1-4} = (2, 1.5, 2, 2)$  and  $g_{a-d} = (12, 20, 50, 100)$  S/F. (—) 4; (----)  $\beta$ ; (-·-·-·) 1; (·····)  $\alpha$ .

For the system in Fig. 8(a), consider the case where  $g_a$  and  $g_c$  were too low to allow 1:1 frequency locking between SN elements 1 and 2 and between 3 and 4, respectively. Then, for  $g_b$  low enough so that SN elements 2 and 3 did not form a single domain, an aperiodic *slow* atrial rhythm resulted. This situation corresponds to that in Fig. 7(b), but with interactions between  $\alpha$  and  $\beta$  via the atrium taken into account, leading to

a total of three domains. When elements 2 and 3 formed one domain—corresponding to the situation where the SN as a whole contains only two domains, one interior and one junctional—the atrial rhythm again followed the bifurcation diagram in Fig. 5(a) as  $g_a-g_c$  increased. Thus, the two-element approximation of a weakly coupled SN seems to be valid even if several SN exit sites are considered.

However, if conduction through one of the exit sites was perfect (1:1), but that through the other was not, it was possible to induce re-entry. For the parameter values given in the figure legend, if the ring was disconnected in the atrial part (b), SN element 1 showed 4:3 Wenckebach conduction with respect to the frequency of elements 2 and 3, which formed a single domain. Their mean firing interval was 368 ms. Element 4 showed 1:1 conduction. Panel (c) shows what occurred in a simulation with an intact ring. When one firing was lost in the Wenckebach cycle of element 1, the impulse transmitted through the exit site to the right re-entered the SN through the left exit site, triggered SN elements 2–4, which sent away a new impulse, and the cycle started over. The re-entrant rhythm persisted indefinitely, with a stable cycle length of 222 ms. It settled for seemingly arbitrary initial conditions. No extra stimulus was needed.

## 4. Discussion

### 4.1. FREQUENCY DOMAINS AND LEAKAGE

The formation of frequency domains seemed to be such a generic phenomenon that if coupling ever becomes so weak that global frequency entrainment is lost, we expect that it arises no matter how peculiar is the SN ultrastructure. However, the splitting into domains seems to be clinically significant only if it occurs close to an SA junction and a severe leakage is assumed. If the splitting occurs far from an exit site, the large peripheral SN domain can drive the atrium at a reasonable rate (Fig. 3). The atrial intervals will also be quite regular, due to the large distance from the domain border (Fig. 1). If leakage is weak, the frequencies of peripheral domains (small or large) can only be slightly decreased and no severe exit blocks can appear. However, if the

peripheral domains are small there will be some atrial interval variations.

In our models, if coupling was generally reduced in the SN, the leakage tended to split the SN into a small, slowly firing domain at the exit sites, and a large normally firing interior one. The main reason for this is that the frequency difference, imposed by the leakage, between SA junctional and interior SN cells was much greater than the variation of natural frequencies between the normal, spontaneous SN cells. If the introduction of connective tissue strands was to have the same effect, they had to be placed close to an exit site, since the borders of domains thus created tended to follow the strand (Fig. 1), and only domains with borders close to exit sites seem to be important, as discussed above.

The appearance of simple exit block rhythms, due to a two-domain situation, did not depend upon some unnatural symmetry of the model system. Natural frequencies were randomly distributed, and connective tissue strands were asymmetrically placed. Thus, we do not think that these phenomena would disappear in more refined models, which more realistically try to mimic the complex SN architecture.

Frequency domains have been observed experimentally in the intestine by Diamant & Borthoff (1969). They registered low-frequency electrical waves in the smooth muscle. If the gut was cut into pieces, the frequency in the pieces gradually decreased moving away from the stomach. In the intact gut, however, the frequency decreased in steps. The situation has been successfully reconstructed using Hodgkin–Huxley-type oscillators coupled in a chain (Patton & Linkens, 1978). In more abstract mathematical oscillator systems, frequency domains have been studied by Sakaguchi *et al.* (1987) and Strogatz & Mirollo (1988). To our knowledge, no attempt has been made to experimentally identify frequency domains in the SN.

#### 4.2. THE INFLUENCE FROM THE ATRIUM

The network system (Fig. 4) in which the atrium was replaced by a constant leakage current showed the same type of dynamics as the one in which the atrium was modelled with excitable elements. The reason why the dynamics of the

atrium in our case had little effect on the SN dynamics are: (1) that sinus rhythm was never so fast that it interfered with the non-automatic element refractory period, and (2) that the atrium was triggered by each SN firing. Thus, even if the current flowing between SN and atrium at the time of an SN firing was far from constant, it was practically the same for each firing of the peripheral SN domain. This can be seen in the leakage current panels in Fig. 2. It did not add new dynamics to the system since it was independent of its history.

#### 4.3. THE TWO-ELEMENT SYSTEM

Since the situation with one normally firing domain in the SN interior and one slowly firing domain at the exit sites was typically present in network simulations, a two-element system was studied in detail. A constant leakage current made the frequency of the junctional element 2 very low if detached from the interior element 1. We could equally well have set the leakage current so high that element 2 lost its automaticity. The main features of the bifurcation diagram [Fig. 5(a)] were preserved nevertheless. The only thing that changed if system parameters were altered seemed to be the integer  $m$  above which the transitions from  $m:1$  to  $(m+1):1$  advanced block became chaotic instead of Wenckebach-like. We note that a bifurcation diagram with the same qualities was obtained if the leakage current was replaced by a row of non-automatic elements.

It is seen in Fig. 5(a), that the 2:1 advanced block region was the widest of those giving imperfect SA conduction. This suggests that this block would be most commonly seen. Among the sick sinus patients studied by Jordan *et al.* (1978), the group with intrinsic SN bradycardia had a mean heart rate after an autonomic blockade of 49 beats  $\text{min}^{-1}$ . This is about half the normal value of around 100 beats  $\text{min}^{-1}$  (Reiffel, 1988). One may speculate that their SNs rested most of the time in the 2:1 block region. For a random parameter choice, the probability of observing an  $(m+1):m$  Wenckebach rhythm decreased with increasing  $m$ . This seems consistent with clinical observations. Rhythms of the type appearing in region  $W_2$  in the bifurcation diagram have been

recorded in periodically stimulated squid giant axons (Takahashi *et al.*, 1990) and also in aggregates of cultured ventricle cells (Soen *et al.*, 1999). It is not known to us whether these, or rhythms of the  $W_3$ -,  $W_4$ - or  $W_5$ - form, have been recorded in sick sinus patients. A 5:2 rhythm in the  $W_2$  class appeared in the network simulations [Fig. 3(c)].

All rhythms appearing in the diagram cannot be expected to be seen clinically in a clean form, because if sinus rhythm is very slow, ectopic beats will be present. Time-dependent nervous influence and coupling conductance fluctuations may also cause sinus rhythm to drift within the diagram. Then transient rhythms will also be seen. In addition, the activity of a frequency domain is not exactly equivalent to that of a single cell.

#### 4.4. LIMITATIONS OF THE TWO-ELEMENT MODEL AND BRADY-TACHY RHYTHMS

Two types of rhythms appearing in network simulations during low intracellular coupling could not be reproduced by the two-element system. The first is aperiodic slow rhythms, which do *not* correspond to the two-element system regions  $C_1$  and  $C_2$  [Fig. 5(a)]. These appeared when the interior SN elements formed more than one frequency domain. This happened, for example, in the system in Fig. 4 for a narrow interval of quite large coupling conductances around  $g_{SS} = 23$  S/F [Fig. 4(e)], and also for the systems in Figs 7 and 8. The other type is the re-entrant tachycardia (Fig. 8), which included both atrial and SN tissue. Re-entry of this type might be one substrate for the brady-tachy syndrome, since it is closely associated with exit block. It requires perfect conduction through one exit site, and some degree of block through another. Consider the system in Fig. 8. If conduction through both exit sites is perfect, a wavefront emanating from one exit site will always meet another one before it can re-enter the SN through the other opening. If conduction through both outlets is imperfect, an impulse emanating from element 4 which is retrogradely conducted through element 1 cannot trigger element 4 anew because, from the premise, it cannot be triggered properly even by two successive normal firings of element 3. In neither case can re-entrant tachycardia be produced.

The exit block ratios of each subsystem may vary with time, so that this critical situation only occurs sometimes. The possibility of a similar kind of re-entry was suggested in the review article by Schuessler *et al.* (1996). It was not too hard to adjust parameters so that the phenomenon appeared. One prerequisite is a slow conduction through the atrial tissue close to the SN, since the retrogradely conducted impulse must enter the SN with sufficient delay so that the interior SN cells are again excitable. One may imagine that the train of re-entrant impulses could induce paroxysms of atrial fibrillation at some critical cycle length. Several studies indicate some connection between the activity of the SN and paroxysmal atrial fibrillation (Kirchhof & Allesie, 1992; Pagé, 1992).

#### 4.5. SCALING CONSIDERATIONS

Throughout this paper, we have used the term “SN element” instead of “SN cell”. We did not fix the scale of our systems, since our aim was to point out possible consequences of poor coupling, not to give parameter values at which different phenomena appear. The coupling level at which the simulated arrhythmias may appear, depends on many factors which we cannot be sure to have modelled accurately: (1) tissue ultrastructure, (2) the ability of SN cells to withstand leakage (model dependent), (3) the attraction of the atrial cell resting state (if this attraction is weak, the SA junctional atrial cells will rest at a higher potential, reducing the leakage), (4) the SA coupling, and (5) atrial coupling (a strong coupling means a strong potential sink of the SA junctional atrial cells, increasing the leakage).

To our knowledge, no one has measured the SA coupling in intact tissue. Joyner *et al.* (1998) found that the lowest coupling at which a model rabbit SN cell could drive a rabbit atrial cell was  $\sim 0.55$  nS. The rabbit SN cell capacitance is  $\sim 50$  pF (Verheijck *et al.*, 1998). Treating the elements of Figs 2 and 3 as actual cells, the chosen value of  $g_{SA} = 100$  S/F corresponds to a safety factor of about ten. Verheule *et al.* (1997) found that the coupling between pairs of rabbit atrial cells ranged from 30 to 635 nS. Our choice of  $g_{AA} = 500$  S/F then corresponds to 25 nS in absolute units, and is certainly too low. The problem

is that with a  $g_{AA}$  corresponding to the mean value of 175 nS of Verheule *et al.* (1997), arrhythmia appeared for a  $g_{SS}$  larger than normal. Here we compared with the mean rabbit SN cell coupling value 2.6 nS found by Anumonwo *et al.* (1992). This points out a quantitative shortcoming of our models.

Regarding the two-element system (Fig. 5), it is clear that each element is intended to represent more than one cell; element 1 corresponds to the whole SN interior, and element 2 to a smaller peripheral domain. Therefore, if  $C$  is the SN cell membrane capacitance, the cell-to-cell conductance,  $g_{cell}$ , is larger than  $gC$ . As an example, imagine that element 2 is cubic and consists of eight smaller isopotential cubic cells. The capacitance of the element is then  $8C$ . Only four of the cells face element 1. Their coupling conductance to element 1 is then  $g_{cell} = g(8C)/4 = 2gC$  each. If three of these cells are disconnected from element 1 due to connective tissue, the conductance of the remaining cell is  $g_{cell} = 8gC$ . Given  $C \sim 50$  pF (Verheijck *et al.*, 1998), and  $g_{cell} \sim 2.6$  nS (Anumonwo *et al.*, 1992), this means that  $g \sim 6.5$  S/F for the “fibrotic” system. It therefore rests close to the  $W_2$ -rhythm region of Fig. 5. This is meant only to show that the rhythms simulated in this paper do not necessarily correspond to unrealistically low conductance values.

#### 4.6. DO THE SIMULATED RHYTHMS APPEAR *IN VIVO*?

The severe arrhythmias simulated in this study can only appear if the leakage to the atrium prevents SA junctional SN cells from driving the atrium by themselves. The strongest indication that this is the case comes from the study by Kirchhof *et al.* (1987). They compared the activity of a rabbit SN preparation before and after disconnection of the CT, and found that the atrium reduced the frequency of the SN *as a whole* by 18% in the mean. This indicates that the activity of SA junctional cells *left alone* would be completely suppressed. Simulation results are inconclusive in this respect. In the model used by Joyner & Van Capelle (1986), an SN of considerable size was needed to drive the atrium, while Boyett *et al.* (1995) found that a single model SN cell could drive an atrial cell no matter how large the SA coupling.

In the simulations we assumed that the SA border is sharp. Physiologically, peripheral SN cells do not seem to be more atrial-like. As mentioned before, their frequencies rather tend to be higher. However, the study by Bleeker *et al.* (1980) indicated that morphologically, myocytes gradually become more atrial-like moving away from the rabbit SN centre. However, later studies of isolated cells have not revealed any intermediate cell types (Denyer & Brown, 1990; Verheijck *et al.*, 1998). A number of immunohistochemical studies (Oosthoek *et al.*, 1993; ten Velde *et al.*, 1995; Kwong *et al.*, 1998; Coppen *et al.*, 1999) have shown a sharp SA border between a Cx43 negative SN and a Cx43 positive atrium.

We also assumed that the impulse leaves the SN at discrete outlets. The review by Schuessler *et al.* (1996) describes how such a view has evolved from more and more detailed mapping of the impulse spread in the atrium. The study by ten Velde *et al.* (1995) also supports this picture, since they found significant SA coupling only at the tips of the atrial strands.

Some experimental studies which can be interpreted as tests of the arrhythmic potential of poor coupling in the SN have already been made. It is known that digitalis may induce sick sinus like arrhythmias. Using rabbit SN preparations, Takayanagi & Jalife (1986) clearly demonstrated that one effect of digitalis is to reduce intercellular coupling. Steinbeck *et al.* (1980) and Takayanagi & Jalife (1986) reported the following time course of the effect of the drug: in right atrial preparations, the firing frequency first gradually increased, then there was a period of irregular, relatively fast firings, then a period of more severe arrhythmia with SA blocks. Finally, the atrium was silent. The early frequency increase was accompanied by a shift of the site of earliest depolarization within the SN from the centre to the periphery. In our view, this stage is most probably due to the gradual uncoupling of the SN from the atrium. The reduced leakage allowed the inherently higher frequency of the SN periphery to be expressed, and it thereby also became the dominant pacemaker site. The effect is the same as that found by Kirchhof *et al.* (1987) when they mechanically disconnected the SN from the atrium. After that, we imagine that the progressing uncoupling inside the SN increased

the net leakage from the SN periphery to the atrium, even though the atrial uncoupling also progressed. The 1:1 entrainment between the SN interior and periphery was lost, and SA blocks developed. In Fig. 7 of Steinbeck *et al.* (1980), it is seen that a peripheral SN fibre is unable to respond to two impulses from the SN interior, creating a transient 3:1 block. It is important to note that the SN interior seems to fire properly, supporting the idea that it is uncoupling alone that causes the arrhythmia.

#### 4.7. POOR COUPLING AND THE SICK SINUS SYNDROME

We wanted to see which rhythm disorders can arise due to poor intercellular coupling in the SN. Given the simulation results, we hypothesize that this condition may be a sufficient cause for most arrhythmias in the sick sinus syndrome. Of course, we do not claim that poor intranodal coupling is the critical condition behind *all* cases of the syndrome. "Poor coupling" may arise in different ways; as a general gap junction decrease due to electro-chemical imbalances; due to an excess of connective tissue strands, or because of areas of inexcitable myocardial cells. They *et al.* (1977) found a significant correlation between the degree of fibrosis in the SN and the occurrence of SA blocks and brady-tachy rhythms. Results by De Mazière *et al.* (1992) suggest that the connective tissue in the SN is electrically insulating, and it therefore probably provides intercellular decoupling.

Some cases of SA blocks due to abnormal nervous influence (Jordan *et al.*, 1978) might be interpreted in the poor coupling scheme. An assumed too large vagal influence, means that peripheral SN cells experience an abnormally large ACh-induced outward current to be added to the hyperpolarizing leakage. Thus, a normal coupling may then be described as too poor to achieve frequency entrainment with an SN periphery subject to this abnormally large load. This case is very similar to the one studied in this paper. The experiments by Slenter *et al.* (1984) showed that while vagal bursts delayed the firings of central rabbit SN cells, the effect on peripheral cells on the septal side was more severe. Sometimes 2:1 or Wenckebach intranodal blocks appeared, where these cells were unable to respond to some stimuli

from the SN interior. In our view, this is due to their larger vulnerability because of the leakage.

The SN recovery time (SNRT) seems to be consistently prolonged among those sick sinus patients who have intrinsic SN disorder (Jordan *et al.*, 1978). If poor coupling is to be the *only* critical condition behind *some* cases of the sick sinus syndrome, this condition in itself must give rise to prolonged SNRT. A recent study showed prolonged SNRT in Cx40-deficient mice (Hagendorff *et al.*, 1999). Two of these also displayed intermittent second-degree SA blocks. Since Cx40 is the dominant gap junction protein in the SN, whereas Cx43 dominates in the atrium (Copen *et al.*, 1999), this is probably an effect purely of poor coupling in the SN. However, one cannot exclude other side effects of the absence of the gene coding for Cx40. We speculate that the cause of the prolonged SNRT in the Cx40-deficient mice is the increased net leakage experienced by peripheral SN cells when coupling is reduced. This makes the diastolic depolarization of these cells more vulnerable to a pacing-induced net outward current.

An increased conductance through the remaining cell-to-cell connections in a fibrotic SN might restore frequency entrainment, as happened with the SN element network with an interaction block in Fig. 1(d). This might also be true for patients with abnormally large vagal influence. However, this would mean supernormal conductances in both cases. To our knowledge, no one has presented a substance which increases the conductance or density of gap junctions.

This study was supported by the Swedish Medical Research Council (grant no. 14X-08664).

#### REFERENCES

- ANUMONWO, J. M. B., WANG, H. Z., TRABKA-JANIK, E., DUNHAM, B., VEENSTRA, R. D., DELMAR, M. & JALIFE, J. (1992). Gap junctional channels in adult mammalian sinus nodal cells: Immunolocalization and electrophysiology. *Circ. Res.* **71**, 229–239.
- BLEEKER, W. K., MACKAAY, A. J., MASSON-PÉVET, M., BOUMAN, L. N. & BECKER, A. E. (1980). Functional and morphological organization of the rabbit sinus node. *Circ. Res.* **46**, 11–22.
- BOYETT, M. R., HOLDEN, A. V., KODAMA, I., SUZUKI, R. & ZHANG, H. (1995). Atrial modulation of sinoatrial pacemaker rate. *Chaos, Solitons & Fractals* **5**, 425–438.

- BOYETT, M. R., HONJO, H., YAMAMOTO, M., NIKMARAM, M. R., NIWA, R. & KODAMA, I. (1999). Downward gradient in action potential duration along conduction path in and around the sinoatrial node. *Am. J. Physiol.* **276**, H686–H698.
- CAI, D., LAI, Y. C. & WINSLOW, R. L. (1993). Complex dynamics in coupled cardiac pacemaker cells. *Phys. Rev. Lett.* **71**, 2501–2504.
- COPPEN, S. R., KODAMA, I., BOYETT, M. R., DOBRZYNSKI, H., TAKAGISHI, Y., HONJO, H., YEH, H. I. & SEVERS, N. J. (1999). Connexin45, a major connexin of the rabbit sinoatrial node, is co-expressed with connexin 43 in a restricted zone at the nodal-crista terminalis border. *J. Histochem. Cytochem.* **47**, 907–918.
- DE HAAN, R. L. (1982). In vitro models of entrainment of cardiac cells. In: *Cardiac Rate and Rhythm* (Bouman, L. N. & Jongsma, H. J., eds), pp. 323–361. The Hague: Nijhoff.
- DELMAR, M., JALIFE, J. & MICHAELS, D. C. (1986). Effects of changes in excitability and intercellular coupling on synchronization in the rabbit sino-atrial node. *J. Physiol.* **370**, 127–150.
- DELON, W. U., YEH, S. J., LIN, F. C., WANG, C. C. & CHERNG, W. J. (1992). Sinus automaticity and sinoatrial conduction in severe symptomatic sick sinus syndrome. *JACC* **19**, 355–364.
- DE MAZIÈRE, A. M. G. L., VAN GINNEKEN, A. C. G., WILDERS, R., JONGSMA, H. J. & BOUMAN, L. N. (1992). Spatial and functional relationship between myocytes and fibroblasts in the rabbit sinoatrial node. *J. Mol. Cell. Cardiol.* **24**, 567–578.
- DENYER, J. C. & BROWN, H. F. (1990). Rabbit sino-atrial node cells: isolation and electrophysiological properties. *J. Physiol.* **428**, 405–424.
- DIAMANT, N. & BORTHOFF, A. (1969). Nature of the intestinal slow-wave frequency gradient. *Am. J. Physiol.* **216**, 301–307.
- FERRER, M. I. (1973). The sick sinus syndrome. *Circulation* **47**, 635–641.
- HAGENDORFF, A., SCHUMACHER, B., KIRCHHOFF, S., LÜDERITZ, B. & WILLECKE, K. (1999). Conduction disturbances and increased atrial vulnerability in connexin40-deficient mice analyzed by transesophageal stimulation. *Circulation* **99**, 1508–1515.
- HODGKIN, A. L. & HUXLEY, A. F. (1952). A quantitative description of membrane current and its application to conduction and excitation in nerve. *J. Physiol.* **117**, 500–544.
- IRISAWA, H. & NOMA, A. (1982). Pacemaker mechanisms of rabbit sinoatrial node cells. In: *Cardiac Rate and Rhythm* (Bouman, L. N. & Jongsma, H. J., eds), pp. 35–51. The Hague: Nijhoff.
- JALIFE, J. (1984). Mutual entrainment and electrical coupling as mechanisms for synchronous firing of rabbit sinoatrial pace-maker cells. *J. Physiol.* **356**, 221–243.
- JAMES, T. N. (1977). The sinus node. *Am. J. Cardiol.* **40**, 965–986.
- JORDAN, J. L., YAMAGUCHI, I. & MANDEL, W. J. (1978). Studies on the mechanism of sinus node dysfunction in the sick sinus syndrome. *Circulation* **57**, 217–223.
- JOYNER, R. W. & VAN CAPELLE, F. J. L. (1986). Propagation through electrically coupled cells: how a small SA node drives a large atrium. *Biophys. J.* **50**, 1157–1164.
- JOYNER, R. W., KUMAR, R., GOLOD, D. A., WILDERS, R., JONGSMA, H. J., VERHEIJCK, E. E., BOUMAN, L., GOOLSBY, W. N. & VAN GINNEKEN, A. C. G. (1998). Electrical interactions between a rabbit atrial cell and a nodal cell model. *Am. J. Physiol.* **274**, H2152–H2162.
- KAPLAN, B. M., LANGENDOREF, R., LEV, M. & PICK, A. (1973). Tachycardia-bradycardia syndrome (so-called “sick-sinus syndrome”). Pathology, mechanisms and treatment. *Am. J. Cardiol.* **31**, 497–508.
- KIRCHHOFF, C. J. H. J. & ALLESSIE, M. A. (1992). Sinus node automaticity during atrial fibrillation in isolated rabbit hearts. *Circulation* **86**, 263–271.
- KIRCHHOFF, C. J. H. J., BONKE, F. I. M., ALLESSIE, M. A. & LAMMERS, W. J. E. P. (1987). The influence of the atrial myocardium, on impulse formation in the rabbit sinus node. *Pflug. Arch.* **410**, 198–203.
- KWONG, K. F., SCHUESSLER, R. B., GREEN, K. G., LAING, J. G., BEYER, E. C., BOINEAU, J. P. & SAFFITZ, J. E. (1998). Differential expression of gap junction proteins in the canine sinus node. *Circ. Res.* **82**, 604–612.
- MICHAELS, D. C., MATYAS, E. P. & JALIFE, J. (1986). Dynamic interactions and mutual synchronization of sinoatrial node pacemaker cells. A mathematical model. *Circ. Res.* **58**, 706–720.
- OOSTHOEK, P. W., VIRÁGH, S., MAYEN, A. E. M., VAN KEMPEN, M. J. A., LAMERS, W. H. & MOORMAN, A. F. M. (1993). Immunohistochemical delineation of the conduction system I: the sinoatrial node. *Circ. Res.* **73**, 473–481.
- OPTHOF, T., VAN GINNEKEN, A. C. G., BOUMAN, L. N. & JONGSMA, H. J. (1987). The intrinsic cycle length in small pieces isolated from the rabbit sinoatrial node. *J. Mol. Cell. Cardiol.* **19**, 923–934.
- OTT, E. (1993). *Chaos in Dynamical Systems*. Cambridge: Cambridge University Press.
- PAGÉ, P. L. (1992). Sinus node during atrial fibrillation: to beat or not to beat? *Circulation* **86**, 334–336.
- PATTON, R. J. & LINKENS, D. A. (1978). Hodgkin–Huxley type electronic modelling of gastrointestinal electrical activity. *Med. Biol. Eng. Comput.* **16**, 195–202.
- REIFFEL, J. A. (1988). Clinical electrophysiology of the sinus node in man. In: *Electrophysiology of the Sinoatrial and Atrioventricular Nodes* (MAZGALEV, T., DREIFUS, L. S. & MICHELSON, E. L., eds), pp. 239–257. New York: Alan R. Liss.
- RUBENSTEIN, J. J., SCHULMAN, C. L., YURCHAK, P. M. & DESANTIS, R. W. (1972). Clinical spectrum of the sick sinus syndrome. *Circulation* **46**, 5–13.
- SAKAGUCHI, H., SHINOMOTO, S. & KURAMOTO, Y. (1987). Local and global self-entrainment in oscillator lattices. *Prog. Theor. Phys.* **77**, 1005–1010.
- SCHUESSLER, R. B., BOINEAU, J. P. & BROMBERG, B. I. (1996). Origin of the sinus impulse. *J. Cardiovasc. Electrophysiol.* **7**, 263–274.
- SLENTER, V. A. J., SALATA, J. J. & JALIFE, J. (1984). Vagal control of pacemaker periodicity and intranodal conduction in the rabbit sinoatrial node. *Circ. Res.* **54**, 436–446.
- SOEN, Y., COHEN, N., LIPSON, D. & BRAUN, E. (1999). Emergence of spontaneous rhythm disorders in self-assembled networks of heart cells. *Phys. Rev. Lett.* **82**, 3556–3559.
- STROGATZ, S. H. & MIROLLO, E. (1988). Phase-locking and critical phenomena in lattices of coupled nonlinear oscillators with random intrinsic frequencies. *Physica D* **31**, 143–168.
- STEINBECK, G., BONKE, F. I. M., ALLESSIE, M. A. & LAMMERS, W. J. E. P. (1980). The effect of ouabain on the

isolated sinus node preparation of the rabbit studied with microelectrodes. *Circ. Res.* **46**, 406–414.

TAKAHASHI, N., HANYU, Y., MUSHI, T., KUBO, R. & MATSUMOTO, G. (1990). Global bifurcation structure in periodically stimulated giant axons of squid. *Physica D* **43**, 318–334.

TAKAYANAGI, K. & JALIFE, J. (1986). Effects of digitalis intoxication on pacemaker rhythm and synchronization in rabbit sinus node. *Am. J. Physiol.* **250**, H567–H578.

THERY, C., GOSELIN, B., LEKIEFFRE, J. & WAREMBOURG, H. (1977). Pathology of sinoatrial node. Correlations with electrocardiographic findings in 111 patients. *Am. Heart J.* **93**, 735–740.

TEN VELDE, I., DE JONGE, B., VERHEIJCK, E. E., VAN KEMPEN, M. J. A., ANALBERS, L., GROS, D. & JONGSMA, H. J. (1995). Spatial distribution of connexin43, the major cardiac gap junction protein, visualizes the cellular network for impulse propagation from sinoatrial node to atrium. *Circ. Res.* **76**, 802–811.

VERHEIJCK, E. E., WESSELS, A., VAN GINNEKEN, A. C. G., BOURIER, J., MARKMAN, M. W. M., VERMEULEN, J. L. M., DE BAKKER, J. M. T., LAMERS, W. H., OPHOF, T. & BOUMAN, L. N. (1998). Distribution of atrial and nodal cells within the rabbit sinoatrial node: models of sinoatrial transition. *Circulation* **97**, 1623–1631.

VERHEULE, S., VAN KEMPEN, M. J. A., TE WELSCHER, P. H. J. A., KWAK, B. R. & JONGSMA, H. J. (1997). Characterization of gap junction channels in adult rabbit atrial and ventricular myocardium. *Circ. Res.* **80**, 673–681.

VICTORRI, B., VINET, A., ROBERGE, F. A. & DROUHARD, J. P. (1985). Numerical integration in the reconstruction of cardiac action potentials using Hodgkin–Huxley-type models. *Comp. Biomed. Res.* **18**, 10–23.

WOHLFART, B. & OHLÉN, G. (1999). Properties of spiral waves in a piece of isotropic myocardium. *Clin. Physiol.* **19**, 11–21.

## APPENDIX A

### A1. Model Specifications

#### A1.1. THE SIMPLIFIED IRISAWA–NOMA MODEL

The currents are given as current densities, in the unit A/F.

$$I/C = Q(i_{Ca} + i_K) + i_h + i_b, \quad (\text{A.1})$$

where  $C$  is the membrane capacitance,  $i_{Na}$  was set to zero and  $Q$  was used to change the natural frequency (Section 2). Normally,  $Q = 1$ . The activation and inactivation variables  $x$  follow

$$dx/dt = \alpha_x(1 - x) - \beta_x x, \quad (\text{A.2})$$

except the Ca-activation  $d$ , which was set to its steady-state value  $d_\infty$ .

$$d = d_\infty = \alpha_d/(\alpha_d + \beta_d). \quad (\text{A.3})$$

Below,  $V$  is assumed to be in millivolts.

$$i_{Ca} = df \times 15(\exp((V - 40)/25) - 1), \quad (\text{A.4})$$

$$\alpha_d = 1.2/(1 + \exp(-V/12)), \quad (\text{A.5})$$

$$\beta_d = 0.25/(1 + \exp((V + 30)/8)), \quad (\text{A.6})$$

$$\alpha_f = 0.0007(V + 45)/\exp((V + 45)/9.5) - 1, \quad (\text{A.7})$$

$$\beta_f = 0.036/(1 + \exp(-(V + 21)/9.5)), \quad (\text{A.8})$$

$$i_K = p \times 0.91(\exp(0.0277(V + 90)) - 1) / \exp(0.0277(V + 40)), \quad (\text{A.9})$$

$$\alpha_p = 0.008/(1 + \exp(-(V + 4)/13)), \quad (\text{A.10})$$

$$\beta_p = 0.00017(V + 40)/\exp((V + 40)/13.3) - 1, \quad (\text{A.11})$$

$$i_h = q(V + 25)/5, \quad (\text{A.12})$$

$$\alpha_q = 0.0034(V + 100)/\exp((V + 100)/4.4) - 1 + 0.0000495, \quad (\text{A.13})$$

$$\beta_q = 0.0005(V + 40)/(1 - \exp(-(V + 40)/6)) + 0.0000845, \quad (\text{A.14})$$

$$i_b = 1.2(1 - \exp(-(V + 60)/25)) + 0.15(V - 2)/(1 - \exp(-(V - 2)/5)). \quad (\text{A.15})$$

#### A1.2. THE WOHLFART–ARLOCK–OHLÉN MODEL

$$I/C = i_{Na} + i_{Ca} + i_K + i_{Kb} \quad (\text{A.16})$$

where  $C$  is the membrane capacitance. The currents are given in A/F. Below,  $V$  is assumed to be in millivolts.

$$i_{Na} = \sigma_{Na} X_{Na} Z_{Na} (V - E_{Na}), \quad (\text{A.17})$$

$$dX_{Na}/dt = k_{Na(a)}(P_{Na(a)} - X_{Na}), \quad (\text{A.18})$$

$$dZ_{Na}/dt = k_{Na(i)}((1 - P_{Na(i)}) - Z_{Na}), \quad (\text{A.19})$$

$$P_{Na(a)} = 1/(1 + \exp(-c_{Na(a)}(V - V_{Na(a)}))). \quad (\text{A.20})$$

$P_{\text{Na}(i)}$  is a function of the same form as  $P_{\text{Na}(a)}$ .  $i_{\text{Ca}}$  is described by equations analogous to those for  $I_{\text{Na}}$ . For the K currents we have

$$i_{\text{K}} = \sigma_{\text{K}} X_{\text{K}} (1 - 3P_{\text{K}}/4)(V - E_{\text{K}}), \quad (\text{A.21})$$

$$i_{\text{Kb}} = \sigma_{\text{Kb}} (1 - 3P_{\text{K}}/4)(V - E_{\text{K}}). \quad (\text{A.22})$$

The dynamical equation for  $X_{\text{K}}$  is analogous to eqn (A.18), and  $P_{\text{K}}$  is of the same form as  $P_{\text{Na}(a)}$ . The following parameter values were used:

---


$$\begin{aligned} E_{\text{Na}} &= 60, & \sigma_{\text{Na}} &= 10, & k_{\text{Na}(a)} &= 1, & V_{\text{Na}(a)} &= -40, & c_{\text{Na}(a)} &= 0.2, \\ E_{\text{Ca}} &= 80, & \sigma_{\text{Ca}} &= 0.04, & k_{\text{Na}(i)} &= 0.27, & V_{\text{Na}(i)} &= -75, & c_{\text{Na}(i)} &= 0.2, \\ E_{\text{K}} &= -90, & \sigma_{\text{K}} &= 0.02, & k_{\text{Ca}(a)} &= 0.1, & V_{\text{Ca}(a)} &= -30, & c_{\text{Ca}(a)} &= 0.2, \\ & & \sigma_{\text{Kb}} &= 0.05, & k_{\text{Ca}(i)} &= 0.02, & V_{\text{Ca}(i)} &= -60, & c_{\text{Ca}(i)} &= 0.2, \\ & & & & k_{\text{K}} &= 0.01, & V_{\text{K}} &= -20, & c_{\text{K}} &= 0.08. \end{aligned}$$